Available online at www.sciencedirect.com
ScienceDirect
Palaeogeography, Palaeoclimatology, Palaeoecology 251 (2007) 254–267
PALAEO
www.elsevier.com/locate/palaeo

The Mediterranean hydrologic budget from a Late Miocene global climate simulation

Rupert Gladstone [a], Rachel Flecker [a,*], Paul Valdes [a], Dan Lunt [a,b], Paul Markwick [c]

[a] *BRIDGE, Geographical Sciences, University of Bristol, University Road, Bristol BS8 1SS, United Kingdom*
[b] *British Antarctic Survey, High Cross, Madingley Road, Cambridge, CB3 0ET, United Kingdom*
[c] *Petroleum Systems Evaluation Group, GETECH, University of Leeds, Leeds, LS2 9JT, United Kingdom*

Received 8 November 2006; received in revised form 2 March 2007; accepted 29 March 2007

Abstract

During the Late Miocene the Mediterranean experienced a period of extreme salinity fluctuations known as the Messinian Salinity Crisis (MSC). The causes of these high amplitude changes in salinity are not fully understood but are thought to be the result of restriction of flow between the Mediterranean and Atlantic, eustatic sea level change and climate. Results from a new Atmospheric General Circulation Model (AGCM) simulation of Late Miocene climate for the Mediterranean and adjacent regions are presented here. The model, HadAM3, was forced by a Late Miocene global palaeogeography, higher CO_2 concentrations and prescribed sea surface temperatures. The results show that fluvial freshwater fluxes to the Mediterranean in the Late Miocene were around 3 times greater than for the present day. Most of this water was derived from North African rivers, which fed the Eastern Mediterranean. This increase in runoff arises from a northward shift in the intertropical convergence zone caused by a reduced latitudinal gradient in global sea surface temperatures. The northwards drainage of the Late Miocene Chad Basin also contributes. Numerical models designed to explore Late Miocene salt precipitation regimes in the Mediterranean, which typically make use of river discharge fluxes within a few tens of percent of present-day values, may therefore be grossly underestimating these fluxes.

Although the AGCM simulated Late Miocene river discharge is high, the model predicts a smaller net hydrologic budget (river discharge plus precipitation minus evaporation) than for present day. We discuss a possible mechanism by which this change in the hydrologic budget, coupled with a reduced connection between the Mediterranean and the global ocean, could cause the salinity fluctuations of the MSC.
© 2007 Elsevier B.V. All rights reserved.

Keywords: General circulation models; Messinian Salinity Crisis; Late Miocene; Mediterranean; North Africa; Rivers

1. Introduction

Semi-enclosed marine basins, particularly those at mid-latitudes, commonly deposit high-resolution, high-amplitude records of past climate. This is because their near landlocked physiography reduces the ocean's buffering effect, rendering the system highly sensitive to regional climatic change. The salinity response of such systems can be extreme. For example, substantial volumes of evaporites lie beneath the seafloor of many of these basins (e.g., Mediterranean, Red Sea, Persian Gulf and Gulf of California) indicating periods in the past when salt concentration was a factor of 3 to 10 times greater than typical oceanic salinity. The salinity of a marginal marine basin is dependent on the basin's

* Corresponding author. Tel.: +44 117 33 17267.
E-mail address: r.flecker@bristol.ac.uk (R. Flecker).

0031-0182/$ - see front matter © 2007 Elsevier B.V. All rights reserved.
doi:10.1016/j.palaeo.2007.03.050

hydrologic fluxes (ocean-basin exchange, and the freshwater budget including evaporation and input from rain and rivers). Studies exploring the mechanisms, amplitude and rate of salinity variation are therefore heavily dependent on accurate hydrologic flux information.

For modern systems, observational information is available to constrain hydrologic budget models, although sparseness of observations can give rise to variation in published fluxes (e.g., Blanc, 2000). Hydrologic flux information for the past is much less easily attainable. Freshwater budget information can be derived from global climate models, but few published general circulation model (AGCM) simulations for the Late Miocene exist (Steppuhn et al., 2006). In the absence of quantitative fresh water budget data, modern data are often used (Flecker et al., 2002; Meijer, 2006).

In the Late Miocene, the Mediterranean experienced extreme salinity fluctuations leading to deposition of evaporite minerals, sediments containing fauna tolerant of normal marine conditions and deposits thought to record fresh-brackish water conditions. This event is known as the Messinian Salinity Crisis (MSC). There are two end-member hypotheses for triggering Late Miocene salt precipitation in the Mediterranean.

1. Desiccation as a result of isolation from the global ocean (Cita, 1982; Hsü et al., 1972, 1973, 1977).
2. Evaporite precipitation under conditions of continued Mediterranean–Atlantic connection (Fabricius and Hieke, 1977), but reduced or negligible Mediterranean outflow and hence enhanced salt concentration.

In both these scenarios, the rate at which salt saturation is reached is controlled by the net rate of freshwater loss, $E-(R+P)$, where E is evaporation over the basin, P is precipitation over the basin, and R is river inflow into the basin. In a desiccating isolated basin, evaporation removes fresh water, concentrating salt in the remaining Mediterranean water. In a basin where outflow is blocked, the net freshwater loss drives the rate of Atlantic water inflow and hence the quantity of salt input to the Mediterranean (Meijer, 2006).

Various approaches have been used to explain the initial salt precipitation in the Late Miocene Mediterranean. First order calculations (Benson and Rakic-El Bied, 1991; Hsü et al., 1973), Sr-salinity modelling (Flecker et al., 2002; Flecker and Ellam, 2006) and box models (Blanc, 2000, 2006; Meijer, 2006; Meijer and Krijgsman, 2005) all rely on modern hydrological flux data. The impact that uncertainties in the water budget have on the results of numerical models of salt precipitation is explored by Blanc (2000); Meijer (2006); and Meijer and Krijgsman (2005). For example, Meijer and Krijgsman (2005) assess the vulnerability of their results to differences between the Late Miocene and present-day freshwater budget by running their model with a ±25% variation in both river discharge and net evaporation. Their results show that the degree of saturation attained in the Eastern Mediterranean is critically dependent on the freshwater budget used.

In this paper we present river discharge and net evaporation information derived from global climate modelling of the Late Miocene using an atmospheric circulation model, HadAM3. We compare model output with available geological evidence and consider its implications for our understanding of salinity fluctuations in the Mediterranean during the Messinian Salinity Crisis.

2. Methods

2.1. Model description

An Atmospheric General circulation Model, AGCM, is a global, three-dimensional, physically based computer model of the climate system. It represents the effects of such factors as reflective and absorptive properties of atmospheric water vapour, greenhouse gas concentrations, clouds, and circulation patterns. We ran

Table 1
Summary of the different sea surface temperature (SST) distributions used as Late Miocene boundary conditions for the AGCM simulations

Experiment	Description of SST construction
Mioc 1	Generated using the sine of the latitude multiplied by a coefficient that varies through the yearly cycle to give a distribution of SSTs that is 2 degrees greater than pre-industrial at the equator, between 4 to 8 degrees warmer at the south pole, and between 6 to 18 degrees warmer at the north pole (depending on time of year)
Mioc 2	Like Mioc 1, but with southern hemisphere SSTs held at equatorial values
Mioc 3	Like Mioc 1, but with uniformly lower SSTs by 2 degrees. This can be thought of as representing some uncertainty in global temperature response to increased CO_2
Mioc 4	Like Mioc 1, but increasing the north pole temperature by 4 degrees
Mioc 5	Like Mioc 1, but changing the latitude of the steepest SST anomaly gradient by squaring the sine function
Mioc 6	Like Mioc 1, but changing the latitude of the steepest SST anomaly gradient by taking the root of the sine function
Mioc 7	Like Mioc 3, but with southern hemisphere SSTs held at equatorial values

These SSTs are represented graphically in Fig. 2.

an AGCM (Pope et al., 2000) with both pre-industrial and Late Miocene boundary conditions. HadAM3 includes global representations of the atmosphere and land surface and is driven by specifying boundary conditions at the top of the atmosphere (incoming radiation) and at the surface (e.g., sea surface

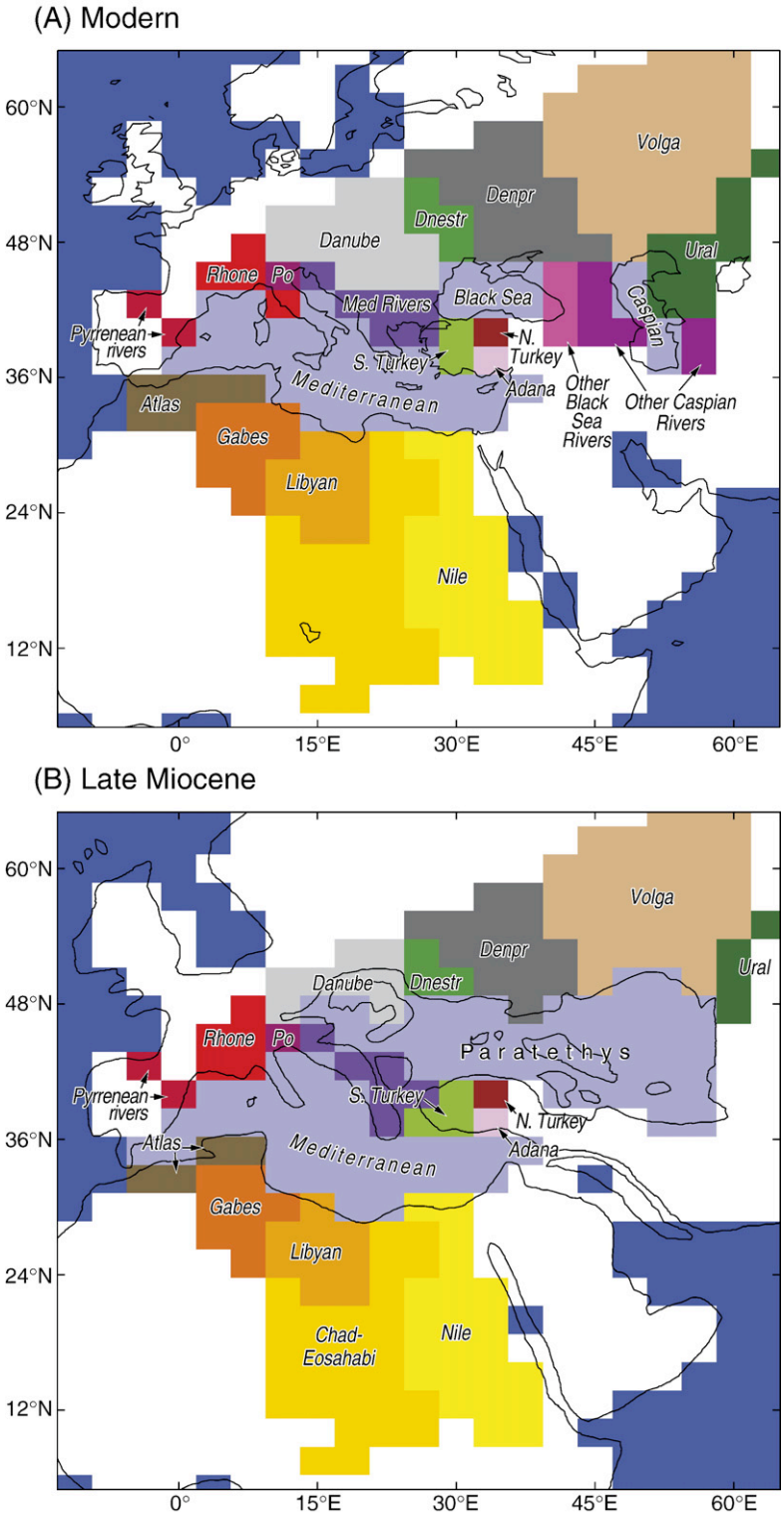

temperature), orography and greenhouse gas concentrations. Land surface properties are either prescribed (e.g., vegetation distribution, soil type) or modelled (e.g., soil moisture, temperature). HadAM3 calculates the time evolution of many climate variables globally at a resolution of 3.75° longitude by 2.5° latitude.

The pre-industrial experimental setup is as documented by Pope et al. (2000), with the following exceptions:

- The means from years 1870 to 1900 of the Hadley centre sea surface temperature (SST) and sea-ice climatologies (HadISST, Rayner et al., 2003) are used. These climatologies are constructed from a variety of sources.
- Vegetation and trace gas concentrations (Dallenbach et al., 2000; Monnin et al., 2001) are as defined by the Paleoclimate Modelling Intercomparison Project stage 2 (PMIP2) requirements (see http://www-lsce.cea.fr/pmip2/). The vegetation distribution is not substantially different from the modern.
- The CO_2 concentration is 278 ppm.

For the Late Miocene experiments, much of the setup, including the orbital forcing, remains the same. The Late Miocene simulations aim to be broadly representative of the Late Miocene rather than a precise replica of the climate for a given moment in time. As such they are intended to capture the major differences between recent and Late Miocene climates. A likely range of Late Miocene climate scenarios is provided by using a range of SST distributions to force the AGCM. In setting up these simulations, three key boundary condition changes have been made from the pre-industrial setup: (1) to the global palaeogeography; (2) the CO_2 concentration, and (3) the sea surface temperatures (SSTs).

(1) The global Late Miocene palaeogeography is that of Markwick et al. (2000). The methodology used to produce this reconstruction is described in detail by Markwick and Valdes (2004) using a Late Cretaceous example. There are several challenges inherent in reconstructing the geography of a past time period including balancing the need for high spatial resolution against the temporal grain of the map, i.e., a high-resolution palaeogeography requires palaeoenvironmental data with a wider range of ages. The nature of that balance depends on the use of the palaeogeographic map (Markwick and Lupia, 2001).

Atmospheric General Circulation Models are relatively insensitive to changes in the palaeogeography. As a result, it is more effective to capture the impacts of palaeogeographic changes during the Late Miocene (e.g., the opening and closing of marine gateways) through changes to the SST structure (Table 1). The Late Miocene palaeogeographic reconstruction we have used therefore tips the balance in favour of high spatial resolution instead of a narrow time period.

A more recent and detailed reconstruction of the Late Miocene Mediterranean coastline and bathymetry has been developed for the purposes of box modelling experiments (Meijer, 2006; Meijer and Krijgsman, 2005; Meijer et al., 2004). On the scale of the grid boxes used to calculate the AGCM (Fig. 1), discrepancies between the two palaeogeographies are insignificant.

(2) The concentrations of trace gases have been changed. Most importantly, CO_2 increases from a pre-industrial value of 278 ppm (parts per million) to a Late Miocene value of 394 ppm (Berner and Kothavala, 2001).

(3) We have modified the sea surface temperature (SST) distribution over the open ocean to reflect the warmer climate of the Late Miocene, driven by a stronger greenhouse effect. Ideally our SST reconstruction would be based on reconstructions from proxy data, but such data for the Late Miocene are sparse, especially for the mid- to high-latitudes. Another recent Late Miocene AGCM modelling study (Steppuhn et al., 2006) uses published planktonic foraminifera $\delta^{18}O$ data from ODP and DSDP sites to construct AGCM boundary conditions. However, as the authors point out there are several difficulties with this approach, such as the effects of post-death diagenesis of the calcareous material (Pearson et al., 2001). Williams et al. (2005) find a discrepancy between SSTs generated using this method, and SSTs constructed using alkenone data, and conclude that a reassessment of diagenetic processes would be needed before using planktonic $\delta^{18}O$ data from many of the ODP/DSDP sites. The proxy evidence for equatorial SSTs lower than today cannot be considered reliable and we therefore construct SSTs for our Late Miocene simulation on a physical basis.

Fig. 1. Map showing (A) modern and (B) Late Miocene drainage basins at the resolution of the general circulation model HadAM3. The Mediterranean, Paratethys, and the Caspian and Black Seas are shown in light blue. Land areas not draining to these seas are un-shaded. The global oceans and other bodies of water are shown in dark blue. The modern coastline (black line) is shown for reference on map (A). The Mediterranean palaeogeography used for the Late Miocene simulation is shown on map (B). Note that the coastlines are shown for reference only. The coastline as used in the simulations is defined by the edge of the blue (ocean) and light blue (sea) regions. (For interpretation of the references to colour in this figure legend, the reader is referred to the web version of this article.)

The structure of the temperature shift between present-day and Late Miocene SSTs is principally determined by consideration of ice-albedo feedbacks. These feedbacks enhance warming relative to the pre-industrial climate in regions that currently are covered in snow or ice and are thus susceptible to enhanced warming through loss of this coverage. Given the uncertainty in exact SSTs, we have constructed seven different SST distributions consistent with this physical argument (Table 1; Fig. 2A), and have run the model for each distribution. As the main results are robust across all these runs (Fig. 3) we simplify the presentation by discussing just the Mioc 1 SST distribution in this paper. The actual zonal mean SST for this run is shown in Fig. 2B.

In all seven cases, the Late Miocene SST distribution is derived by adding a seasonally and latitudinally varying anomaly to the pre-industrial SST distribution.

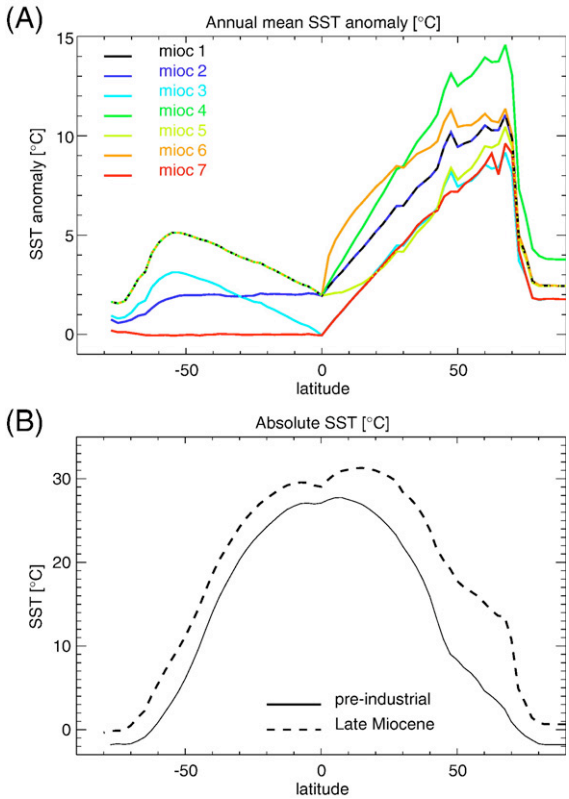

Fig. 2. (A) Zonal mean of the annual mean SST anomalies added to the pre-industrial SST distribution to provide SSTs for the Late Miocene simulations. Note that smooth functions were used in the first stage of generating these anomalies, and the jagged appearance (mostly at high latitudes) results from the changed geography and sea-ice distributions (see text). The simulation discussed in the text uses SST anomaly Mioc 1. (B) Zonal absolute SST distribution for pre-industrial and Late Miocene (Mioc 1) simulations.

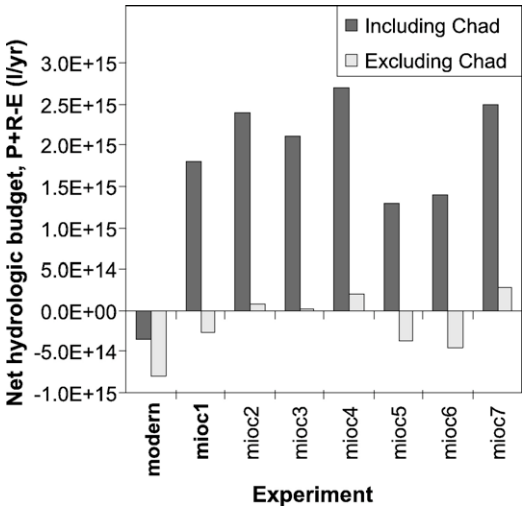

Fig. 3. Drainage into the Eastern Mediterranean for all simulations, including and excluding Chad drainage. The Miocene simulations forced by different SST distributions (Fig. 2A) all show greatly increased drainage from North Africa to the Eastern Mediterranean, and much of this increase is due to increased precipitation over the Chad Basin. The simulations used in most of the discussion are indicated in bold text.

The anomaly, based on a sine function of latitude, is always either zero or positive, so Miocene SSTs are always at least as warm as those of the pre-industrial simulation. The anomaly:

- increases towards the poles, leading to a decrease in the meridional temperature gradient;
- is greatest in winter seasons, and
- is greater in the Northern Hemisphere than the Southern Hemisphere (Fig. 2A).

The seven different SST anomalies used in our experiments are summarised in Table 1 and Fig. 2A. Experiments Mioc 3 and 7 can be thought of as representing some uncertainty in the global temperature response to increased CO_2. Experiments Mioc 4, 5 and 6 represent a range of northern hemisphere latitudinal SST gradients and high latitude change. Together these experiments represent a likely range of Late Miocene SST anomalies based on physical arguments which are consistent with data that indicate increased northern hemisphere SSTs (Pearson et al., 2001; Steppuhn et al., 2006).

Certain coastal SSTs have to be extrapolated due to the discrepancy between the modern and Late Miocene land–sea masks. Where the Late Miocene SST is colder than the freezing point of water, sea-ice is allowed to form, and the surface temperature is no longer prescribed

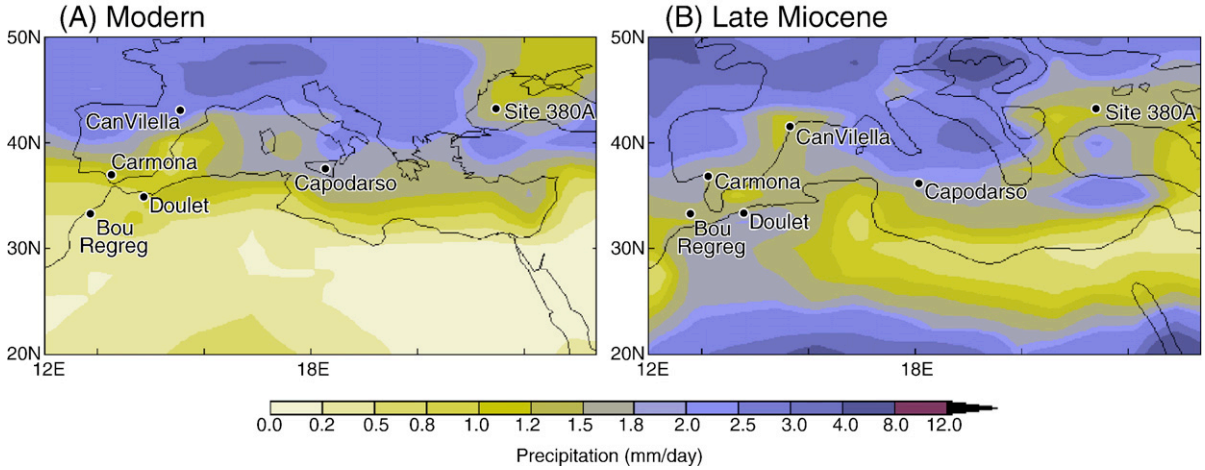

Fig. 4. Precipitation over the Mediterranean and surrounding regions, as simulated by HadAM3 for (A) the pre-industrial and (B) the Late Miocene periods. Modern and Late Miocene reconstructed (Markwick et al., 2000) coastlines are shown. Note that the scale is non-linear. The locations of pollen data used in model–data point comparisons (Fig. 8) are shown.

but is computed by the AGCM. This results in a reduced sea-ice coverage compared to present day. A reduced Greenland ice sheet also constitutes a part of the Late Miocene model setup. The resulting absolute ocean surface temperatures, including under sea-ice, in the pre-industrial and Late Miocene are shown in Fig. 2B.

2.2. Model validation

Since HadAM3 is a physics-based model, validation for one time period improves confidence in the model's performance for other time periods, provided the forcing is realistic. HadAM3 was used in the first phase of PMIP (Joussaume and Taylor, 1995), to simulate mid-Holocene (6 kyr BP) and Last Glacial Maximum (LGM, 21 kyr BP) climates. In common with all the PMIP AGCMs, HadAM3 simulates some aspects of Quaternary climates well and some less well. For example, it does a good job of simulating LGM annual mean temperature and precipitation changes over Europe, but underestimates the LGM winter cooling over western Europe (Jost et al., 2005; Kageyama et al., 2001). In addition, HadAM3 has been used to simulate several pre-Quaternary climates, including a study of the Pliocene climate of Europe and the

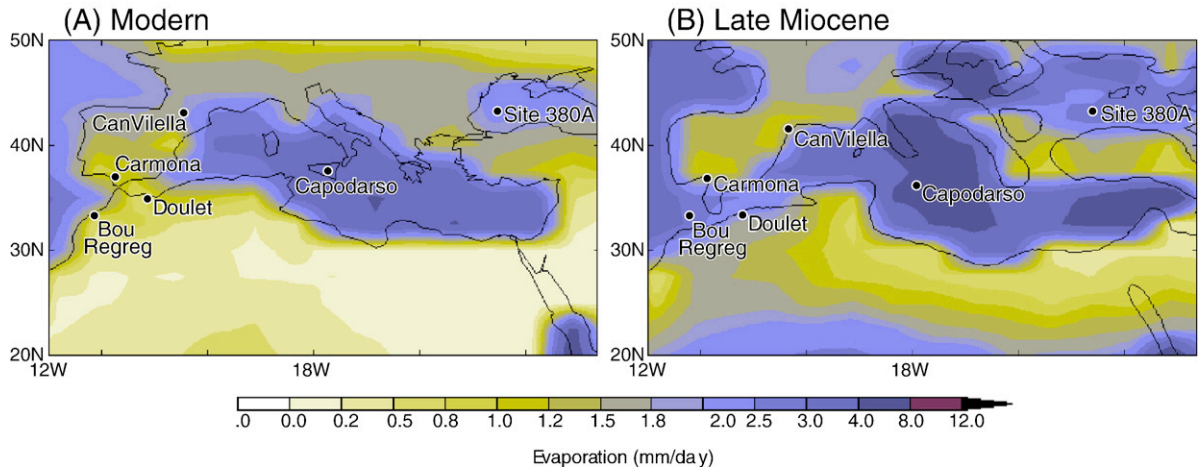

Fig. 5. Evaporation (e.g., total loss of water from the surface to the atmosphere, including sublimation and transpiration) over the Mediterranean and surrounding regions, as simulated by HadAM3 for (A) the pre-industrial and (B) the Late Miocene periods. Coastlines are as in Fig. 3. Note that the scale is non-linear.

Table 2
Late Miocene and modern river discharge (Vorosmarty et al., 1998)

River basin/water masses		Modern discharge	HadAM3 simulated modern discharge	Simulated 8 Ma discharge
		l/year	l/year	l/year
Seas	Mediterranean		−2.1e+15	−2.5e+15
	Paratethys			−2.1e+15
	Black Sea		−2.2e+14	
	Caspian		−1.7e+14	
Drains into Eastern Mediterranean	Eonile Basin	4.0e+13	2.2e+14	9.2e+14
	Chad Basin*	Does not drain into Mediterranean		2.1e+15
	Eosahabi Basin*	0.0e+00	6.6e+11	1.5e+13
	Libyan Basin*	0.0e+00	3.8e+12	3.6e+13
	Gabes Basin*	0.0e+00	5.1e+12	1.3e+13
	Adana	6.9e+12	7.9e+11	9.8e+12
	Po	4.8e+13	1.7e+14	5.4e+12
	Turkey south	No information	8.4e+12	2.9e+13
	Turkey west	3.1e+12	8.1e+12	1.1e+14
Drains into Western Mediterranean	Atlas*	2.0e+12	1.1e+13	8.4e+12
	Rhone	5.3e+13	1.4e+13	1.5e+14
	South Pyrrenean rivers	2.3e+13	4.3e+13	1.6e+13
Drains into Caspian (Paratethys)	Ural	9.4e+12	1.6e+14	1.1e+14
	Other rivers	No information	6.1e+12	6.4e+13
	Volga	2.6e+14	2.5e+13	
Drains into Black Sea (Paratethys)	Dnepr	4.7e+13	3.3e+14	1.2e+15
	Other rivers	No information	1.8e+14	3.9e+14
	Dnestr	1.2e+13	5.9e+13	
	Danube	2.0e+14	7.0e+13	1.2e+14
	Turkey north	1.2e+13	4.6e+14	2.5e+14
Net freshwater budget ($P-E+R$)	Mediterranean including Chad drainage		−1.0e+15	8.6e+14
	Mediterranean excluding Chad drainage			−1.2e+15

North African rivers west of the Nile are indicated by "*".

Mediterranean (Haywood et al., 2000) which showed close agreement between the model results and proxy data derived from the geological record.

2.3. Processing model outputs

Amongst many other climate variables, HadAM3 output fields include total precipitation (Fig. 4)[1] and total evaporation (including evapo-transpiration; Fig. 5). These data are provided on the 3.75° × 2.5° model grid. Each of the Late Miocene simulations was run for 20 years, and in each case the outputs described here are calculated from an average of the last 15 years.

In order to calculate net hydrologic fluxes over the basins draining to the Mediterranean, the model grid cells must all be assigned to drainage basins (Fig. 1). The Messinian drainage basins for North Africa west of the Nile are defined by Griffin (2002), who, in accord with other authors (e.g., Orszag-Sperber et al., 1993), suggests that the physiography of North Africa has not changed greatly since the Late Miocene. These river courses are thought to have been incised during Messinian draw-down of Mediterranean sea level (Barr and Walker, 1973). All other drainage basins are defined on the basis of modern drainage patterns. To calculate the drainage rates into the Mediterranean from each basin (Table 2), the total evaporative loss integrated over the basin was subtracted from the total precipitation integrated over the basin (Fig. 6). This is valid given that over the long-term, soil moisture equilibrates in the land surface component of the model.

3. Results

The Late Miocene simulation shows net precipitation ($P-E$) across most of the Mediterranean region similar to that of the control run (i.e., present day), with evaporation exceeding precipitation particularly strongly in

[1] All the model results from our pre-industrial and Late Miocene simulations, including many variables not directly discussed in this paper, are available online, at http://www.bridge.bris.ac.uk/resources/simulations. A username and password are available on request from the corresponding author.

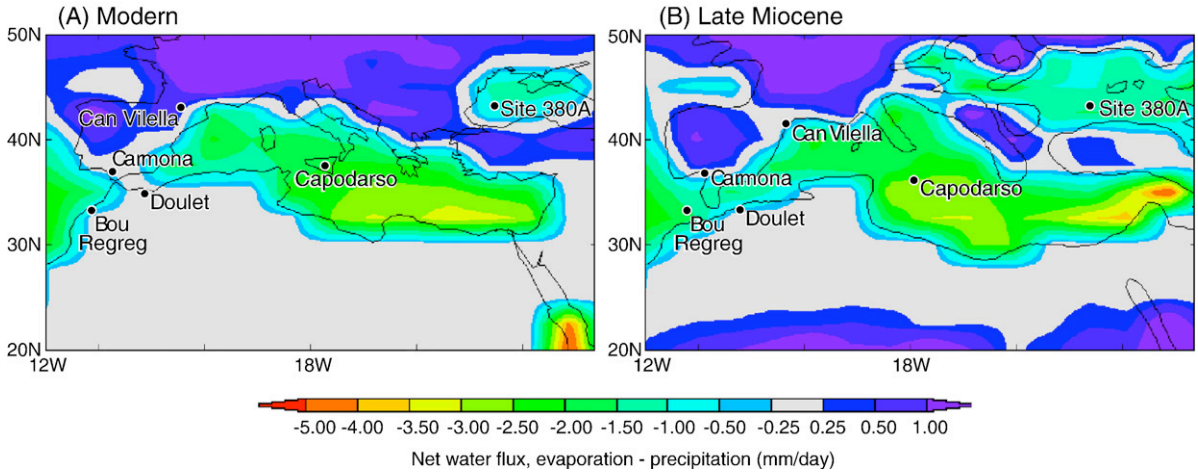

Fig. 6. Net flux of water from the atmosphere to the land (or sea) surface over the Mediterranean and surrounding regions, as simulated by HadAM3 for (A) the pre-industrial and (B) the Late Miocene periods. Coastlines are as in Fig. 3. Note that the scale is non-linear.

the Eastern sub-basin (Fig. 6). The major difference between the two time intervals occurs in North Africa where modelled $P-E$ (and indeed both precipitation and evaporative water loss separately) is much higher in the Late Miocene (Figs. 4–6). The difference is most pronounced in northern Central Africa (south of 25°N), well to the south of the Mediterranean coast. Much of this region of increased net precipitation is over North African Messinian river catchments that drained north into the Mediterranean (Fig. 1), but because of low rainfall today do not flow at all. According to our simulation, this increase in net precipitation in the Late Miocene caused increased river inflow to the Eastern Mediterranean. The amount of fresh water reaching the Eastern Mediterranean was substantially enhanced by the large Chad Basin catchment area which drained northward during the Late Miocene (Griffin, 2002; Griffin, 2006).

Today, the Chad Basin is a region of internal drainage with low drainage divides to the southwest via the Benue River to the Niger Delta. Griffin (2002) points out that since the Messinian, the southern fluvial divides of the Chad Basin have been subject to considerable erosion and are probably now significantly lower than they were 5–6 million years ago. By contrast, the northern drainage divides have been preserved by the area's prevalent aridity. In his 2002 paper, Griffin traces large-scale fluvial features across northern Chad and Libya, linking the Chad Basin with a prominent fluvial incision feature preserved near the Gulf of Sirt on the coast of Libya. A brief summary of the evidence that supports this interpretation is presented here.

Griffin (2002) interprets the fluvial incision features found along the north coast of Africa as having been generated as a result of Mediterranean base-level fall during the MSC and he maintains that the magnitude of this incision records the magnitude of river flow at the time. The Gulf of Sirt channel is associated with sediments that contain a rich freshwater biota including large reptiles. The habitat of these creatures requires large bodies of water (e.g., lakes or very substantial river systems, Hecht, 1987). Griffin argues that although these sediments are Pliocene, because of the Messinian age of the incision and the decreasing rainfall that

Table 3
Late Miocene and modern discharge into the Eastern and Western Mediterranean sub-basins and the Caspian and Black Sea sub-basins of Paratethys in l/year

Discharge basin			Modern observations	Simulated modern river discharge	Simulated modern $P+R-E$	Simulated Late Miocene river discharge	Simulated Late Miocene $P+R-E$
Mediterranean	Eastern	With Chad	9.7e+13	4.5e+14	−1.5e+15	3.2e+15	8.6e+14
		Without Chad				1.1e+15	−1.2e+15
	Western		7.9e+13	1.8e+14	−6.5e+14	1.7e+14	−9.2e+14
Paratethys	Caspian		2.6e+14	3.3e+14	1.1e+14	1.3e+15	−5.5e+13
	Black Sea		2.8e+14	7.3e+14	5.6e+14	7.7e+14	

characterises the transition from Messinian–Pliocene (as interpreted from dust records for example, e.g., deMenocal and Bloemendal, 1995), the river that supported early Pliocene crocodiles was also present during the Messinian. Griffin then uses satellite imagery to trace this Eosahabi River southwards to the East Tibetsi Valley where a channel feature ~5 km wide is visible. In searching for a large volume water source to generate this channel, Griffin concludes that since there is no visual evidence that it was derived from the Niger to the west, or the monsoonal rains of Ethiopia to the east, it must have come from the south. Griffin rules out the Congo as a more southerly source than the Chad Basin area because of the tectonic divide between the two and suggests instead that during the Neogene, subsidence in the Chad Basin (Genik, 1993) favoured lake formation when the $P-E$ relationship permitted, just as occurred during the Pleistocene/Holocene (Pachur and Altmann, 1997).

Fig. 3 highlights the importance of the Chad drainage basin in terms of the hydrologic budget of the Eastern Mediterranean but demonstrates that a Late Miocene net precipitation increase relative to the present day is a robust result across our set of simulations forced by different SST distributions (Fig. 3). In summary, although the net evaporation across the Mediterranean in the Late Miocene was similar to today, the amount of freshwater supplied to the Mediterranean was substantially larger 8 million years ago (Table 3; Fig. 7).

This modelled increase in North African rainfall is due to increased latitudinal migration of the Intertropical Convergence Zone (ITCZ). The ITCZ is the region where the northeasterly and southeasterly tradewinds converge, forming an often continuous band of clouds or thunderstorms. It oscillates latitudinally with the season, driven by changing surface temperatures which are themselves forced by incoming solar radiation. The northward extent of the ITCZ during the northern hemisphere summer is limited by the pattern and strength of latitudinal gradients of surface temperature.

Previous climate model studies have simulated shifts in the ITCZ. For example, evidence suggests there was greater rainfall over most of the Sahara during the mid-Holocene. This was probably caused by a northwards shift in the ITCZ in response to orbital forcing and enhanced by ocean and vegetation feedbacks. The increase is reproduced in GCM simulations, although fully coupled atmosphere–ocean–vegetation models (AOVGCMs) more closely match the data than AGCMs, which tend to underestimate the response (Joussaume et al., 1999; Peyron et al., 2006). Our

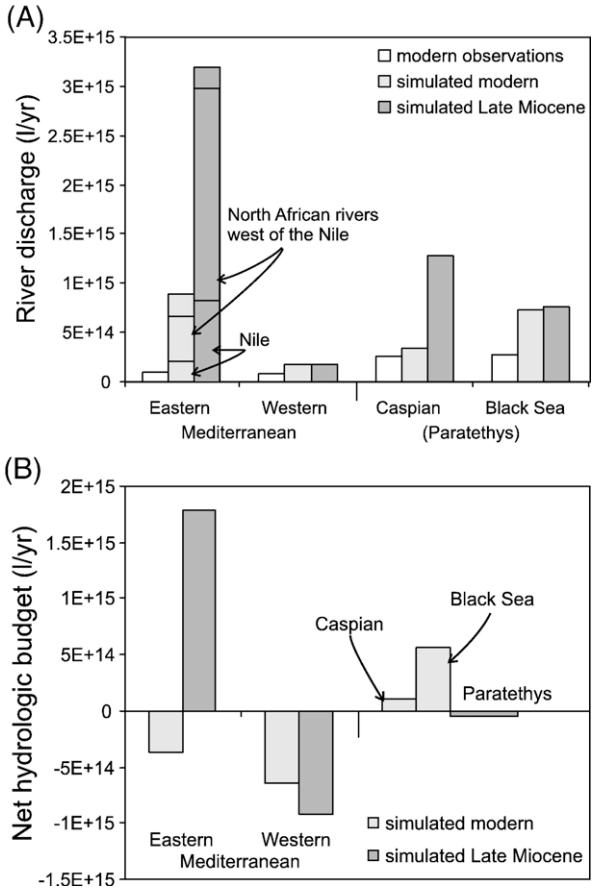

Fig. 7. (A) Empirical estimates for modern river run-off (Vorosmarty et al., 1998) compared with simulated pre-industrial and Late Miocene run-off values. The river systems used to estimate Late Miocene discharge to the Caspian and Black seas were the same as those that exist today; in the Late Miocene however, these rivers fed a single Paratethyan sea. (B) Histogram of the simulated pre-industrial and Late Miocene net hydrologic budgets (precipitation + river discharge − evaporation) for the Mediterranean. Chad Basin discharge is included in the Late Miocene net hydrologic budget for the Eastern Mediterranean. The values used to generate these in charts are shown in Tables 2 and 3.

prescribed SST distributions (Table 1; Fig. 2) aim to represent the oceanic response to a warmer Late Miocene climate, with enhanced polar warming due to the ice-albedo feedback. This is not entirely dissimilar in nature to the change in latitudinal SST gradient due to the mid-Holocene orbital forcing, although it is larger in magnitude. In the Late Miocene simulation, the decreased latitudinal temperature gradient in the prescribed SSTs (Fig. 2A) allows the ITCZ to move further from the equator, providing a large positive net $P-E$ over the North African basins that drain into the Mediterranean. Today, the ITCZ is confined further south, so these North African rivers are currently dry.

Fig. 7A plots both modern run-off data from global river discharge datasets (Vorosmarty et al., 1998) and our model-simulated present-day run-off. While there is reasonable agreement between the real and simulated discharge to the Western Mediterranean and Caspian today, there is a considerable discrepancy in discharge to the Eastern Mediterranean and to a lesser extent the Black Sea (Fig. 7A). This discrepancy is probably in part the result of limitations in our surface run-off calculation which neglects the evaporation from the surface of rivers, instead transporting run-off instantaneously to the ocean. It may also be caused by the fact that the model prescribes rather than simulates the oceans; as a result the hydrologic budget may not be closed, permitting overestimation of precipitation. Whatever the cause of these discrepancies in modern real and simulated discharge volumes, the largest of them (Eastern Mediterranean) is small by comparison with the difference between Late Miocene and modern discharge (Fig. 7A). Since the mechanism for increased Late Miocene North African river discharge, migration of the ITCZ, is distinct from the suggested causes of modern overestimation, although some caution should be exercised over the absolute discharge figures the model produces, the trend towards much higher discharge in the Late Miocene Eastern Mediterranean is robust. For the purposes of restricting bias, all comparisons between modern and Late Miocene climate parameters use modern fluxes provided by the atmospheric simulation.

4. Evaluation and discussion

Direct validation of the model against Late Miocene climate data is desirable, however quantitative climate data are sparse on a global scale. Confidence in the model stems in large part from modern and other paleo model–data comparisons (discussed in 2.2 above) and from more local comparisons (discussed below).

4.1. Data for validation of modelled Late Miocene Mediterranean climate

As well as the presence of large river courses of Messinian age, there is plenty of other qualitative evidence to support a moist climate over North Africa during the Late Miocene (Table 4). Some of the most compelling evidence comes from offshore cores in the Arabian Sea (deMenocal and Bloemendal, 1995) and North Atlantic (Ruddiman et al., 1989) which record low dust fluxes from North Africa at this time. In addition, large Messinian sediment pulses characterise the successions recovered from the Red Sea, Gulf of Suez (Griffin, 1999) and on the Nile Delta (Said, 1993).

Assessing whether the climatic output from the model in the Mediterranean region is numerically realistic is more challenging since quantitative climate data with which to compare model output are limited to a few pollen sites around the Mediterranean (Fauquette et al., 2006). Even where these data are available comparison with model output is problematic. Pollen information is derived from a point source (core) and therefore reflects the immediate local environment. By contrast, the model output is derived from the grid box whose centre is closest to the core location and reflects an average value for that grid box (an area in the order of 10^5 km^2). The error bars on the pollen data are large, reflecting uncertainties in the method of derivation (Fig. 8). As a result, only extreme conflicts between model output and these pollen data would be significant. In this instance, discrepancies where they exist are small (Fig. 8). One area where this approach might be more effective is

Table 4
Qualitative evidence for wet north African climate during the Late Miocene (from Griffin, 2002)

Data	Evidence	Reference
River canyons and courses across North Africa	Thought to have incised during the MSC draw-down and would have required significant river erosion	Griffin (1999)
Dust records	Low dust flux from west Africa to the North Atlantic indicate a wet climate in Africa that became wetter between 8 and 5 Ma	Ruddiman et al. (1989)
	Ocean Drilling Project cores in the Arabian Sea indicate increased monsoonal activity	deMenocal and Bloemendal (1995)
Sediment accumulation	Large Messinian sand pulse in the Red Sea and Gulf of Suez indicating vigorous fluvial activity in the region	Griffin (1999)
	20% of all Nile delta deposits since its inception 6 million years ago are Messinian.	Said (1993)
Humic material	Land-derived humic material at Tokar on Red Sea coast indicates rapid deposition from vegetated areas, in keeping with high rain fall	Bunter and Abdel Magid (1989)
Karstification	Profound subaerial karstification of the Egyptian Red Sea coast may have occurred during Messinian or more recently	El Aref (1993); Griffin (1999)

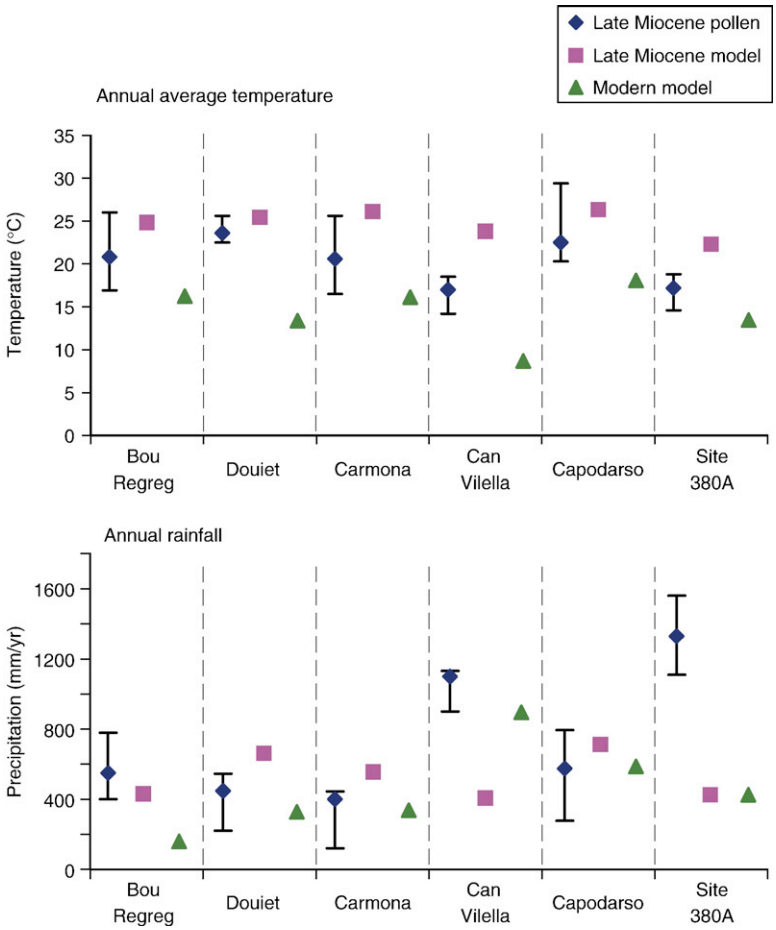

Fig. 8. Model–data comparison. Temperature and precipitation values for the locations shown in Fig. 3, reconstructed from pollen data (Fauquette et al., 2006), are shown (with error bars). Also plotted are the modelled temperature and precipitation values for the grid cell whose centre is closest to the observation point (errors not quantifiable).

North Africa (south of the coastal regions) where the largest difference between modern and Late Miocene precipitation is located (Fig. 4). Regrettably there are currently no published Late Miocene pollen sites in North Africa.

4.2. Implications of large freshwater discharge into the Eastern Mediterranean

Fig. 7 indicates that total river discharge into the Mediterranean and Paratethys (the vast lacustrine precursor to the Black and Caspian Seas, Fig. 1) during the Late Miocene was considerably greater than it is today. The 25% variation incorporated into some box models and used to assess the impact of uncertainties in the freshwater budget (Meijer, 2006; Meijer and Krijgsman, 2005) amply accommodates changes in discharge to the Western Mediterranean but fails to capture the ~3-fold increase in Late Miocene discharge relative to present-day river run-off in the Eastern Mediterranean (Table 3). This difference in behaviour is because almost all the extra Late Miocene rain water was routed to the Mediterranean through North African rivers (Fig. 7A; Table 2) and drained into the Eastern Mediterranean (Table 3; Fig. 1). As a result of this substantial freshwater supply, the hydrologic budget for the Eastern Mediterranean in the Late Miocene was both large and positive (Fig. 7B). This contrasts with a relatively small decrease in the net hydrologic budget for the western Mediterranean (Fig. 7B). Model output suggests that the rivers supplying the Black Sea and Caspian today fed more run-off into Paratethys in the Late Miocene (Fig. 7A). Although our model does not incorporate a Paratethyan–Mediterranean connection (Fig. 1), if exchange were possible at this time (Snel et al., 2006), this Paratethyan water

would also have fed the Eastern Mediterranean. Models of salinity change in the Mediterranean which subdivide the system into its western and eastern sub-basins therefore need to adjust the net hydrologic budget to the eastern basin.

The AGCM results suggest that the components of the Mediterranean freshwater budget, evaporation and freshwater inflow (precipitation plus river inflow), were larger during the Late Miocene than at present (Figs. 4 and 5). In spite of this, the net freshwater budget in the Mediterranean (precipitation [P]+river discharge [R]−evaporation [E]) was of the same order of magnitude in the Late Miocene as today (Table 2). Hence the net freshwater budget, and indeed its sign, may have been more sensitive to climatic changes during the Late Miocene than at present.

Reduced exchange between the global ocean and semi-enclosed marine basins, like the Mediterranean, results in an amplified response to changes in the hydrologic balance of the marginal marine system (Thunell et al., 1988). If the connection between the Mediterranean and global ocean was highly restricted as is postulated for the Messinian Salinity Crisis, only very small climatic changes would be needed to switch between hypersaline conditions suitable for precipitating evaporites and the much lower salinity conditions represented by normal marine sediments (e.g., Braga et al., 2006; Riding et al., 1998) or the fresh and brackish environments that characterise Lago Mare deposits (Cita et al., 1990; Orszag-Sperber et al., 2000).

In the scenario of a shallow connection too restricted to allow both a significant inflow and outflow from and to the global ocean (Meijer and Krijgsman, 2005), a small negative net freshwater budget ($E>P+R$) would drive a small positive inflow of global ocean water. Without any outflow this inflow would lead to increasing salinity of Mediterranean water and eventually, evaporite precipitation. A small positive net freshwater budget ($P+R>E$) under similar circumstances would drive an outflow to the Atlantic and result in freshening of at least the upper levels of the Mediterranean water column.

Given a certain degree of natural climatic variability we anticipate that if, over time, the mean net fresh water budget is close to zero but negative (driving a positive inflow from the ocean), there will be occasional intervals when the Mediterranean experiences positive net freshwater budget conditions, reversing the flow direction. These temporary outflows allow salt export to the Atlantic, reducing the salinity of Mediterranean water.

Thus the sensitivity of Mediterranean salinity to reversals in the sign of the hydrologic budget is greatly increased when the connectivity with the global ocean drops low enough that significant inflow and outflow cannot occur simultaneously. A small (but non-zero) connection between the Mediterranean and global ocean therefore provides us with a potential explanation for the high amplitude salinity fluctuations that are documented in the Mediterranean's Late Miocene geological record where evaporites are overlain by or interbedded with much lower salinity sediments be they marine (Riding et al., 1998) or brackish (Fortuin and Krijgsman, 2003; Krijgsman et al., 2001).

5. Conclusions

Output from an atmospheric global climate model suggests that the Mediterranean received considerably more fresh water from river discharge and rainfall in the Late Miocene than it does today. Most of this extra freshwater derives from rainfall across northern central Africa resulting from a northward migration of the Intertropical Convergence Zone. This water reached the Eastern Mediterranean via rivers that no longer run today, but whose courses are well preserved (Griffin, 2002, 2006).

Although the absolute discharge values should be treated with caution, they do have implications for numerical models designed to simulate Late Miocene salt precipitation in the Mediterranean as the result of greatly increased freshwater drainage to the Eastern Mediterranean is robust. These models typically use modern hydrologic flux data and test sensitivity to uncertainty in the Late Miocene fresh water budget by varying modern values by a few tens of percent, which our simulations suggest is inadequate for the Eastern Mediterranean.

Model output also indicates that Late Miocene net fresh water budget for the Mediterranean was closer to zero than today. In association with a restricted gateway to the Atlantic, this would have made the Mediterranean more vulnerable to small climatic changes which have an amplified impact on salinity. Potentially, this may provide a mechanism for the high amplitude salinity variations recorded in the geology of the Messinian Salinity Crisis.

Acknowledgements

The manuscript has benefited from the helpful reviews of Paul Meijer and an anonymous reviewer. The authors acknowledge useful discussions with

Katerina Michaelides and Paul Bates. Jon Tooby helped draft the figures. The computer time required to run these simulations was provided by NCAS.

References

Barr, F.T., Walker, B.R., 1973. Late Tertiary channel system in Northern Libya and its implications on Mediterranean sea level changes. In: Ryan, W.B.F., Hsu, K.J., et al. (Eds.), Initial Reports of the Deep Sea Drilling Project, pp. 1244–1251.

Benson, R.H., Rakic-El Bied, K., 1991. An important current reversal (influx) in the Rifian corridor (Morocco) at the Tortonian–Messinn Boundary: the end of Tethys Ocean. Paleoceanography 6 (1), 164–192.

Berner, R.A., Kothavala, Z., 2001. GEOCARB III: a revised model of atmospheric CO_2 over phanerozoic time. American Journal of Science 301 (2), 182–204.

Blanc, P.-L., 2000. Of sills and straits: a quantitative assessment of the Messinian Salinity Crisis. Deep-Sea Research 47, 1429–1460.

Blanc, P.L., 2006. Improved modelling of the Messinian Salinity Crisis and conceptual implications. Palaeogeography, Palaeoclimatology, Palaeoecology 238 (1–4), 349–372.

Braga, J.C., et al., 2006. Testing models for the Messinian Salinity Crisis: the Messinian record in Almeria, SE Spain. Sedimentary Geology 188–9, 131–154.

Bunter, M.A.G., Abdel Magid, A.E.M., 1989. The Sudanese Red Sea: 2. New developments in petroleum geochemistry. Journal of Petroleum Geology 12, 167–186.

Cita, M.B., 1982. The Messinian Salinity Crisis in the Mediterranean: a review. Alpine-Mediterranean Geodynamics: Geodynamics Series 7, 113–140.

Cita, M.B., Santambrogio, S., Melillo, B., Rogate, F., 1990. Messinian paleoenvironments: new evidence from the Tyrrhenian Sea (ODP Leg 107). In: Kastens, K.A., Mascle, J., et al. (Eds.), Proceedings of the Ocean Drilling Program, Scientific Results.

Dallenbach, A., et al., 2000. Changes in the atmospheric CH4 gradient between Greenland and Antarctica during the Last Glacial and the transition to the Holocene. Geophysical Research Letters 27 (7), 1005–1008.

deMenocal, P.B., Bloemendal, J., 1995. Plio-Pleistocene climatic variability in subtropical Africa and the paleoenvironment of Hominid evolution: a combined data–model approach. In: Vrba, E., Denton, G.H., Partricge, T.C., Burckle, L.H. (Eds.), Paleoclimate and Evolution with Emphasis on Human Origins. Yale University Press, New Haven, pp. 262–288.

El Aref, M., 1993. Paleokarst surfaces in the Neogene succession of Wadi Essel - Wadi Sharm El Bahari area, Egyptian Red Sea coast; as indication of uplifting and exposure. In: Philobbos, E.R., Purser, B.H. (Eds.), Geodynamics and Sedimentation of the Red Sea- Gulf of Aden Rift System. Geological Society of Egypt, pp. 205–231. Special publication.

Fabricius, F.H., Hieke, W., 1977. Neogene to Quaternary development of the Ionian Basin (Mediterranean): considerations based on a "dynamic shallow basin model" of the Messinian salinity event. In: Biju-Duval, B., Montadert, L. (Eds.), Structural History of the Mediterranean Basins. Editions Technip, Paris, pp. 391–400.

Fauquette, S., et al., 2006. How much did climate force the Messinian Salinity Crisis? Quantified climatic conditions from pollen records in the Mediterranean region. Palaeogeography, Palaeoclimatology, Palaeoecology 238, 281–301.

Flecker, R., Ellam, R.M., 2006. Identifying late Miocene episodes of connection and isolation in the Mediterranean–Paratethyan realm using Sr isotopes. Sedimentary Geology 188–189, 189–203.

Flecker, R., de Villiers, S., Ellam, R.M., 2002. Modelling the effect of evaporation on the salinity-$^{87}Sr/^{86}Sr$ relationship in modern and ancient marginal-marine systems: the Mediterranean Messinian Salinity Crisis. Earth and Planetary Science Letters 203 (1), 221–233.

Fortuin, A.R., Krijgsman, W., 2003. The Messinian of the Nijar Basin (SE Spain): sedimentation, depositional environments and paleogeographic evolution. Sedimentary Geology 160, 213–242.

Genik, G.J., 1993. Petroleum geology of Cretaceous-Tertiary rift basins in Niger, Chad and Central African Republic. American Association of Petroleum Geologists Bulletin 77, 1405–1434.

Griffin, D.L., 1999. The late Miocene climate of Northeastern Africa: unravelling the signals in the sedimentary succession. Journal of the Geological Society of London 156, 817–826.

Griffin, D.L., 2002. Aridity and humidity: two aspects of the late Miocene climate of North Africa and the Mediterranean. Palaeogeography, Palaeoclimatology, Palaeoecology 182, 65–91.

Griffin, D.L., 2006. The late Neogene Sahabi rivers of the Sahara and their climatic and environmental implications for the Chad Basin. Journal of the Geological Society 163, 905–921.

Haywood, A.M., Sellwood, B.W., Valdes, P.J., 2000. Regional warming: Pliocene (3 Ma) paleoclimate of Europe and the Mediterranean. Geology 28 (12), 1063–1066.

Hecht, M., 1987. Fossil snackes and crocodilians from the Sahabi Formation of Libya. In: Boaz, N.T., El-Arnauti, A., Gaziry, A.W., de Heinzelin, J., Boaz, D.D. (Eds.), Neogene Paleontology and Geology of Sahabi, Libya. Liss, New York, pp. 101–106.

Hsü, K.J., Cita, M.B., Ryan, W.B.F., 1972. The origin of the Mediterranean evaporites. In: Ryan, W.B.F., Hsü, K.J. (Eds.), Initial Reports of the Deep Sea Drilling Project. US Government Printing Office, Washington D.C., pp. 1203–1231.

Hsü, K., Ryan, W.B.F., Cita, M.B., 1973. Late Miocene desiccation of the Mediterranean. Nature 242, 240–244.

Hsü, K.J., et al., 1977. History of the Mediterranean salinity crisis. Nature 267, 399–403.

Jost, A., et al., 2005. High-resolution simulations of the last glacial maximum climate over Europe: a solution to discrepancies with continental palaeoclimatic reconstructions? Climate Dynamics 24 (6), 577–590.

Joussaume, S., Taylor, K., 1995. Status of the Paleoclimate Modelling Intercomparison Project (PMIP). Proceedings of the First international AMIP Scientific Conference, Monterrey, California, USA, pp. 425–430.

Joussaume, S., et al., 1999. Monsoon changes for 6000 years ago: results of 18 simulations from the Paleoclimate Modeling Intercomparison Project (PMIP). Geophysical Research Letters 26 (7), 859–862.

Kageyama, M., et al., 2001. The last glacial maximum climate over Europe and western Siberia: a PMIP comparison between models and data. Climate Dynamics 17, 23–43.

Krijgsman, W., Fortuin, A.R., Hilgen, F.J., Sierro, F.J., 2001. Astrochronology for the Messinian Sorbas basin (SE Spain) and orbital (precessional) forcing for evaporite cyclicity. Sedimentary Geology 140 (1–2), 18.

Markwick, P.J., Lupia, R., 2001. Palaeontological databases for palaeobiogeography, palaeoecology and biodiversity: a question of scale. In: Crame, J.A., Owen, A.W. (Eds.), Palaeobiogeography and Biodiversity Change: A Comparison of the Ordovician and

Mesozoic–Cenozoic Radiations. Geological Society of London, pp. 169–174.

Markwick, P.J., Valdes, P.J., 2004. Palaeo-digital elevation models for use as boundary conditions in coupled ocean-atmosphere GCM experiments: a Maastrichtian (Late Cretaceous) example. Palaeogeography, Palaeoclimatology, Palaeoecology 213, 37–63.

Markwick, P., et al., 2000. Late Cretaceous and Cenozoic global palaeogeographies: mapping the transition from a "hot-house" world to an "ice-house" world. Geologiska i Stockholm Gorehandlingar 122 (1), 103.

Meijer, P., 2006. A box model of the blocked-outflow scenario for the Messinian Salinity Crisis. Earth and Planetary Science Letters 248 (1–2), 486–494.

Meijer, P., Krijgsman, W., 2005. A quantitative analysis of the desiccation and re-filling of the Mediterranean during the Messinian Salinity Crisis. EPSL 240, 510–520.

Meijer, P.T., Slingerland, R., Wortel, M.J.R., 2004. Tectonic control on past circulation of the Mediterranean sea: a model study of the late Miocene. Paleoceanography 19, 1026.

Monnin, E., et al., 2001. Atmospheric CO_2 concentrations over the last glacial termination. Science 291 (5501), 112–114.

Orszag-Sperber, F., et al., 1993. Atlas tethys palaeoenvironmental maps. In: Dercourt, J., Ricou, L.E., Vrielynck, B. (Eds.), Maps. BEICIP-FRANLAB, Rueil-Malmaison.

Orszag-Sperber, F., Rouchy, J.-M., Blanc-Valleron, M.-M., 2000. La transition Messinien–Pliocene en Mediterranee orientale (Chypre): la periode du Lago-Mare et sa signification. Comptes Rendus de l'Académie des Sciences Paris, Sciences de la Terre et des planetes 331, 483–490.

Pachur, H.-J., Altmann, N., 1997. The Quaternary (Holocene ca. 8000 a BP). In: Schandelmeier, H., Reynolds, O.-O. (Eds.), Palaeogeographic-Palaeotectonic atlas of North-Eastern Africa, Arabia and Adjacent Areas, Balkema, Rotterdam, pp. 111–125.

Pearson, P.N., et al., 2001. Warm tropical sea surface temperatures in the Late Cretaceous and Eocene epochs. Nature 413, 481–487.

Peyron, O., et al., 2006. Quantitative reconstructions of annual rainfall in Africa 6000 years ago: model–data comparison. Journal of Geophysical Research 111 (D24110), 1–9.

Pope, V.D., Gallani, M.L., Rowntree, P.R., Stratton, R.A., 2000. The impact of new physical parametrizations in the Hadley Centre climate model: HadAM3. Climate Dynamics 16 (2–3), 123–146.

Rayner, N.A., et al., 2003. Global analyses of sea surface temperature, sea ice, and night marine air temperature since the late nineteenth century. Journal of Geophysical Research 108 (D14, 4407), 1–37.

Riding, R., Braga, J.C., Martin, J.M., SanchezAlmazo, I.M., 1998. Mediterranean Messinian Salinity Crisis: constraints from a coeval marginal basin, Sorbas, southeastern Spain. Marine Geology 146 (1–4), 1–20.

Ruddiman, W.F., et al., 1989. Late Miocene to Pleistocene evolution of climate in Africa and the low-latitude Altantic: overview of Leg 108 results. In: Ruddiman, W.F., Sarnthein, M., et al. (Eds.), Proceedings of the Ocean Drilling Program, Scientific Results, pp. 463–464.

Said, R., 1993. The River Nile. Geology, Hydrology and Utilization. Pergamon Press, Oxford.

Snel, E., Marunteanu, M., Macalet, R., Meulenkamp, J.E., N, v.V., 2006. Late Miocene to early Pliocene chronostratigraphic framework for the Dacic Basin, Romaina. Palaeogeography, Palaeoclimatology, Palaeoecology 238 (1–4), 107–124.

Steppuhn, A., Micheels, A., Geiger, G., Mosbrugger, V., 2006. Reconstructing the late Miocene climate and oceanic heat flux using the AGCM ECHAM4 coupled to a mixed-layer ocean model with adjusted flux correction. Palaeogeography, Palaeoclimatology, Palaeoecology 238, 399–423.

Thunell, R.C., Locke, S.M., Williams, D.F., 1988. Glacio-eustatic sea-level control on Red Sea salinity. Nature 334, 601–604.

Vorosmarty, C.J., Fekete, B.M., Tucker, B.A., 1998. Global river discharge, 1807–1991 Version 1.1 (RivDis). Dataset. Available online [http:www,daac,ornl.gov] from Oak Ridge National Laboratory distributed Active Archive Centre, oak Ridge, Tennessee, USA.

Williams, M., Haywood, A.M., Hillenbrand, C.D., Wilkinson, I.P., 2005. Efficacy of delta O-18 data from Pliocene planktonic foraminifer calcite for spatial sea surface temperature reconstruction: comparison with a fully coupled ocean-atmosphere GCM and fossil assemblage data for the mid-Pliocene. Geological Magazine 142 (4), 399–417.